https://doi.org/10.5194/bg-2021-81
Preprint. Discussion started: 6 April 2021

Biogeosciences Discussions
Open Access

Field-scale CH_4 emission at a sub-arctic mire with heterogeneous permafrost thaw status

Patryk Łakomiec[1], Jutta Holst[1], Thomas Friborg[2], Patrick Crill[3], Niklas Rakos[4], Natascha Kljun[5], Per-Ola Olsson[1], Lars Eklundh[1], Janne Rinne[1]

[1] Department of Physical Geography and Ecosystem Science, Lund University, 223 62, Sweden

[2] Department of Geosciences and Natural Resource Management, University of Copenhagen, 1165, Denmark

[3] Department of Geological Sciences and Bolin Centre for Climate Research, Stockholm University, 114 19, Sweden

[4] Abisko Scientific Research Station, Swedish Polar Research Secretariat, Abisko, 981 07, Sweden

[5] Centre for Environmental and Climate Science, Lund University, 223 62, Sweden

Correspondence to: Patryk Łakomiec (patryk.lakomiec@nateko.lu.se)

Abstract

The Artic is exposed to faster temperature changes than most other areas on Earth. Constantly increasing temperature will lead to thawing permafrost and changes in the CH_4 emissions from wetlands. One of the places exposed to those changes is the Abisko-Stordalen Mire in northern Sweden, where climate and vegetation studies have been conducted from the 1970s.

In our study, we analyzed field-scale methane emissions measured by the eddy covariance method at Abisko-Stordalen Mire for three years (2014-2016). The site is a subarctic mire mosaic of palsas, thawing palsas, fully thawed fens, and open water bodies. A bimodal wind pattern prevalent at the site provides an ideal opportunity to measure mire patches with different permafrost statuses with one flux measurement system. The flux footprint for westerly winds is dominated by elevated palsa plateaus, while the footprint is almost equally distributed between palsas and thawing bog-like areas for easterly winds. As these patches are exposed to the same climatic conditions, we analyzed the differences in the responses of their methane emission for environmental parameters.

The methane fluxes followed a similar annual cycle over the three study years, with a gentle rise during spring and a decrease during autumn and with no emission burst at either end of the ice-free season. The peak emission during the ice-free season differed significantly for the mire with two permafrost statuses: the palsa mire emitted 24 mg-CH_4 m^{-2} d^{-1} and the thawing wet sector 56 mg-CH_4 m^{-2} d^{-1}. Factors controlling the methane emission were analyzed using generalized linear models. The main driver for methane fluxes was peat temperature for both wind sectors. Soil water content above the water table emerged as an explanatory variable for the three years for western sectors and the year 2016 in the eastern sector. Water table level showed a

https://doi.org/10.5194/bg-2021-81
Preprint. Discussion started: 6 April 2021

significant correlation with methane emission for the year 2016 as well. Gross primary production, however, did not show a significant correlation with methane emissions.
Annual methane emissions were estimated based on four different gap-filing methods. The different methods generally resulted in very similar annual emissions. The mean annual emission based on all models was 4.2 ± 0.4 g-CH_4 m^{-2} a^{-1} for western sector and 7.3 ± 0.7 g-CH_4 m^{-2} a^{-1} for the eastern sector. The average annual emissions, derived from this data and a footprint climatology, were 3.6 ± 0.7 g-CH_4 m^{-2} a^{-1} and 11 ± 2 g-CH_4 m^{-2} a^{-1} for the palsa and thawing surfaces, respectively. Winter fluxes were relatively high, contributing 27 - 45 % to the annual emissions.

1 Introduction

After a period of stabilization in the late 1990s to early 2000s, atmospheric methane (CH_4) concentration is increasing again at rates similar to those before 1993, which is approximately 12 ppb yr^{-1} (Dlugokencky et al. 2011, Nisbet et al. 2014, Saunois 2020). The reasons behind this increase are not clearly understood, as the mechanisms that control the global CH_4 budget are not completely comprehended (Kirschke et al. 2013, Saunois et al. 2020). The largest natural source of CH_4 is wetlands, based on top-down emission estimates (Saunois et al. 2020), and this source may be become stronger in the warming climate (Zhang et al. 2017). The shift in the isotopic composition of CH_4 towards more negative values also supports the hypothesis of changes in the biological source strength driving the increase in methane concentration, as atmospheric CH_4 is becoming more ^{13}C-depleted (Nisbet et al. 2016).

Increasing temperature has shown to speed up the degradation of permafrost which leads to losses in the soil carbon pool, often in the form of carbon dioxide (CO_2) and CH_4 (Malmer et al. 2005). The high northern latitudes are experiencing the fastest temperature increase due to the ongoing global warming. Temperature changes in the Arctic have been twice as high as the global average (Post et al. 2019).

Ecosystems near the annual 0°C isotherms are vulnerable to permafrost thaw and changes in ecosystem characteristics in a warming climate. These vulnerable ecosystems include palsa mires, such as Stordalen Mire near Abisko, Sweden, where the recent warming has led to annual average temperatures exceeding 0°C since 1998 (Callaghan et al. 2010, Post et al. 2019, Figure S1). The warming has led to an acceleration of permafrost thaw processes and a transition from palsa plateaus, underlain by permafrost, to non-permafrost fen systems (Malmer et al. 2005). These deviations are likely to induce changes in biogeochemical processes, including increased CH_4 emissions (Christensen et al. 2003).

The most direct micrometeorological field-scale method used to measure CH_4 exchange between ecosystem and atmosphere is the eddy covariance (EC) method (e.g. Verma et al. 1986, Aubinet et al., 2012). The advantages of this method are its high temporal resolution and minimal disturbance to the measured surface. Thus, it is feasible for long-term measurements of rates of gas exchange that integrates over surface variation (Knox et al. 2016, Li et al. 2016, Rinne et al.

https://doi.org/10.5194/bg-2021-81
Preprint. Discussion started: 6 April 2021

2018). However, information on the small-scale spatial distribution of surface fluxes is lost with the method due to the spatially integrative nature of the EC method. Instead of resolving the small-scale spatial variability, the EC method provides averaged fluxes from a larger area, the flux footprint area (Kljun et al. 2015). However, spatial variability can be resolved by the EC method using measurements conducted under different wind directions, as the footprint area is located upwind of the measurement tower. We can take advantage of this feature to obtain gas exchange rates from two different ecosystem types with one measurement system by placing the measurement system on the border between these systems (e.g. Jackowicz-Korczyński et al., 2010; Kowalska et al., 2013; Jammet et al., 2015; 2017). Stordalen Mire offers an excellent opportunity to conduct flux studies where one flux system is used to monitor two ecosystem types since the wind direction is bimodal. While previous studies in the area have compared open water surfaces to completely thawed fen (Jammet et al., 2015, 2017, Jansen et al. 2020), no comparison of field-scale CH_4 emission between permafrost palsa plateaus and thawing wet areas has been conducted.

Previous studies on CH_4 emission within the Stordalen Mire from areas with different permafrost statuses have been done by chamber measurements (McCalley et al. 2014, Deng et al. 2014). McCalley et al. (2014) reported CH_4 emissions from palsas underlain by permafrost to be close to zero, summertime emissions from thawing wet areas to be around 35 mg-CH_4 m^{-2} d^{-2}, while completely thawed fen sites revealed much higher emission of 210 mg-CH_4 m^{-2} d^{-2}. There are only a few wintertime data on CH_4 emission available using the chamber method (Christensen et al. 2000, Nilsson et al. 2008, Godin et al. 2012, McCalley et al. 2014). However, EC measurements conducted at different northern mires typically show low but positive emissions in winter (Rinne et al., 2007; Yamulki et al. 2013, and others).

In this study we analyzed field-scale CH_4 emission from two areas of Stordalen subarctic mire. The first area is dominated by permafrost plateau, while the second one is thawing, wetter areas. Outputs from this analysis are differences in the CH_4 emissions from the mire patches with heterogeneous permafrost status. We are expecting, based on the previous studies, that fluxes from the wetter sector will be around 40 mg-CH_4 m^{-2} d^{-2}, while palsa plateau will emit significantly lower fluxes during a peak season. We presume that winter fluxes will be positive but very low.

For estimation of annual CH_4 emission we need gap-free data-sets. As there at the moment exists no generally accepted gap-filling method for methane fluxes, four different gap-filling methods were compared. All of these methods are uncertain and dealing with the gaps differently. Test of the four methods will decrease the uncertainty in an annual balance estimation. It was important to use more than one method in this case of study because datasets were portioning and due to that contained more gaps.

This study aimed to estimate the annual CH_4 emission from two distinct different ecotypes, with heterogeneous permafrost status, exposed to the same environmental factors. Furthermore, we analyzed the seasonal cycle of CH_4 emission to quantify the contribution during different seasons.

https://doi.org/10.5194/bg-2021-81
Preprint. Discussion started: 6 April 2021

Moreover, an analysis of differences in controlling factors for these two different areas will be done.

2 Materials and method

2.1 Measurement site

The study area is Stordalen Mire, a mire complex underlain by discontinuous permafrost located in northern subarctic Sweden (68^{o}20’ N, 19^{o}30’ E) near Abisko (Ábeskovvu). The station Abisko-Stordalen (SE-Sto) is a part of the ICOS Sweden research infrastructure and is the only one situated in the subarctic region in Sweden. The measurement period that is analyzed here covers three years from 2014 to 2016. The mean annual temperature in this region has been increasing during the last decades and temperatures recorded by SMHI (Sveriges meteorologiska och hydrologiska institut) at ANS (Abisko Naturvetenskapliga Station) has exceeded the 0^{o}C threshold since the late 1980s (Callaghan et al. 2013, Figure S1). During the years 2014-2016, the mean annual air temperature (Ta) was 1.03°C and 0.27°C at ANS and the ICOS Sweden station Abisko-Stordalen (SE-Sto), respectively. The annual precipitation, based on ANS data, is around 330 mm yr^{-1}. An acceleration of permafrost loss with increasing temperatures is likely (Callaghan et al. 2013).

The large mountain valley of Lake Torneträsk (Duortnosjávri) channels winds at the measurement site, leading to a bimodal wind distribution (Figure 1) that allows us to divide our analyses into two distinct sectors. The plant community structure around the tower is determined by the hydrology which in turn is determined by the microtopographic variation in the surface due to the local permafrost dynamics. Different plant communities would have different productivities thus controlling the CO_2 and CH_4 fluxes from those surfaces. The area to the west of the EC mast is dominated by a drier permafrost palsa plateau hereafter referred to as the western sector, whereas the area to the east is a mixture of thawing wet areas and palsas, hereafter referred to as the eastern sector. The drained permafrost plateau is dominated by *Empetrum hermaphroditum*, *Betula nana*, *Rubus chamaemorus*, *Eriophorum vaginatum*, *Dicranum elongatum*, *Sphagnum fuscum*. The wet areas are characterizing by *E. vaginatum*, *Carex rotundata*, *S. balticum*, *Drepanucladus schulzei*, *Politrichum jensenii* (Johansson et al. 2006). The thawing areas in this sector exhibit ombrotrophic, bog-like, features. Dominant vegetation varies with the microforms of the mire.

Figure 1. The wind rose for SE-Sto tower for years 2014-2016 for the daytime (left panel) and nighttime (right panel)

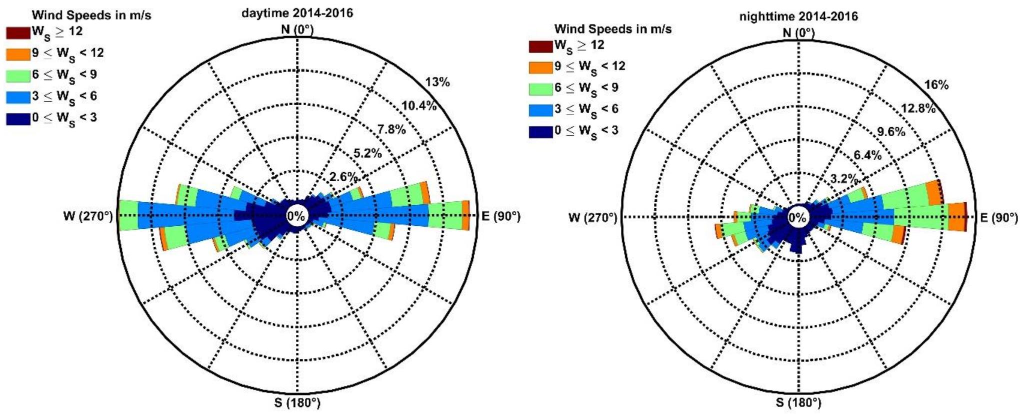

2.2 Flux measurements

The EC measurements of CH_4 fluxes at SE-Sto are made using a close-path fast off-axis integrated cavity output spectrometer (OA-ICOS LGR model GGA-24EP, ABB Ltd, Zurich, Switzerland) combined with a 3-D sonic anemometer (SA-Metek uSonic-3 CLASS A, Metek GmbH, Germany). Air was sampled via a 29.6 m long polyethylene tubing with an 8.13 mm inner diameter. The nominal tube flow rate was 36 l min^{-1}. The sampling inlet was displaced 22 cm horizontally of the sonic anemometer measurement volume towards 180°. The response time of the LGR-FGGA was 0.1 s. The LGR FGGA was placed inside a heated and air-conditioned shelter. The anemometer was located north of the instrument shelter and was oriented with the sensors north pointing towards 186°. This orientation allows undisturbed wind measurements from both main wind directions, East and West.

CO_2 and H_2O were measured with Licor LI-7200 (LICOR Environment, USA) closed path infra-red gas analyzer. The sampling inlet was at the same location as the sampling point for the CH_4 analyzer. Sampled air was transported through 1.05 m and of 5.3 mm ID tubing. The nominal tube flow rate was 15 l min^{-1}.

The anemometer and air sampling tubes were mounted on a mast of 2.2 m a.g.l. (68°21'21.32"N, 19° 2'42.75"E), placed on the edge of the western and the eastern sectors. Data were collected by an ISDL data logger (In Situ Instrument AB, Sweden) with a 20 Hz time resolution.

2.3 Ancillary Measurements

Ancillary measurements are presented in Table S1. The sampling frequency for these parameters was 1 Hz and the collected data were averaged into half-hourly values. Measured variables are divided into two categories: peat/soil parameters, and meteorological parameters. Peat temperatures at each depth, soil heat fluxes, and soil water contents (SWC) were measured at four plots around the EC tower, located towards the four cardinal directions. In further analysis, data just from two of these locations were used (East and West) as these were within the flux footprints areas of the EC tower. The sites for the water table level (WTL) measurements differed from the peat temperature profiles. Furthermore, data for WTL was available only during the unfrozen period, as the probes were removed during the frozen period to avoid damage. The WTL on the western sector was measured in a wet collapse feature, surrounded by drained areas. The palsa areas commonly have no persistent WTL above the permafrost surface. Meteorological variables were measured on a separate mast, placed 10 meters south-west of the flux measurement mast.

2.4 Flux calculation

Fluxes of CO_2, CH_4, H_2O, and sensible heat were calculated using EddyPro 6.2.1 (LICOR Environment, USA) as half-hourly averages. The data quality flagging system and advanced options for EddyPro were set up following Jammet et al. (2017). The wind vector was rotated by a double rotation method and data were averaged by block averaging (Aubinet et al. 2012). The time lag was obtained by maximizing the covariance (Aubinet et al. 2012).

Based on the wind direction, the half-hourly data were divided into western and eastern datasets, similarly to analyses by Jackowicz-Korczyński et al. (2010) and Jammet et al. (2015, 2017). The eastern dataset contained fluxes and other variables recorded when the wind was from 45°-135°, and the western dataset parameters when wind directions were 225°-315°. These two datasets were analyzed separately. Fluxes measured with wind from these two sectors are influenced by mire surfaces dominated by differing permafrost status, moisture regimes, and plant community structures. These reflect the thaw stages of a dynamic arctic land surface, responding to the warming climate. These two wind sectors cover more than 80 % of all data during the years 2014-2016. Northerly and Southerly wind directions, i.e. winds from outside these sectors occurred mainly in low wind speed conditions. The distribution of wind directions is presented in Figure 1.

CH_4 fluxes were filtered by quality flags according to Mauder and Foken (2004). These indicate the quality of measured fluxes, “0” being the best quality fluxes, “1” being usable for annual budgets, and “2” being flux values that should not be used for any analysis. Thus, in further analysis fluxes with flag “2” were removed. Also, flux values when two consecutive data points originated from different wind direction sectors were removed. We also analyzed the behavior of the CH_4 fluxes against low turbulence conditions using friction velocity (u*) as a measure of turbulence. We binned the CH_4 fluxes into 0.05 m s^{-1} u* bins and plotted the binned CH_4 flux values against u* in 40-day windows over the growing period (d.o.y. 150-250, d.o.y. 210 was the beginning of the last averaging window). The CH_4 flux showed no dependence on u* below 0.6 m s^{-1}. A slight positive correlation was found during stronger turbulent conditions (u* > 0.6 m s^{-1}), but we deemed this not high enough to warrant exclusion of those points from further analysis. Thus, we removed no data based on the results of u*. The fraction of data remaining,

https://doi.org/10.5194/bg-2021-81
Preprint. Discussion started: 6 April 2021

after filtering based on the quality flags and other criteria described above, is presented in Table 3.

The analysis of relations of CH_4 fluxes to environmental parameters was done using non-gap-filled dataset of daily averages, to avoid the danger of circular reasoning of analyzing the relations to the same factors that were be used for gap-filling.

2.5 Footprint modeling and land cover classification

Footprint calculation was made with the model described by Kljun et al. (2015). Receptor height, Obukhov length, a standard deviation of lateral velocity fluctuations, friction velocity, and roughness length were used as input data. The input data were divided into the two sectors mentioned above, before footprint calculation, and footprints were calculated separately for them. We calculated footprints for each half-hourly data point and aggregated these to annual footprint climatologies for each sector separately.

A detailed land cover classification was performed over the EC-tower footprint to estimate the flux contribution from the drained palsa and the thawing wet areas. We used images over the Stordalen Mire collected with an eBee (SenseFly, Lausanne, Switzerland) Unmanned Aerial Vehicle (UAV) carrying a Parrot Sequoia camera (Parrot Drone SAS, Paris, France) on July 31, 2018. The images were processed in Agisoft Photoscan (Agisoft LLC, St. Petersburg, Russia) to create an orthomosaic and a Digital Surface Model (DSM) with spatial resolutions of 50 x 50 cm. Field data for training a classification were collected in mid-August 2018 with sampling areas of 50 × 50 cm that were classified into wet or dry, and a random forest classification was performed to classify the footprint into wet and dry areas with the orthomosaic and DSM as input. The dry areas in the flux footprint areas of SE-Sto footprint correspond to palsas, while the wet areas are thawing surfaces.

Based on the land cover classification and annual CH_4 fluxes for each sector, combined and weighted with the footprint climatolgy, it was possible to estimate annual emissions from the different surface type.

2.6 Gap-filling methods for CH_4

We compared four different gap-filling methods, separately for both sectors. These methods were: look-up tables (REddyProc ("Jena gap-filling tool"), Wutzler et al. 2018), 5-day moving mean, artificial neural network (Jammet et al. 2015,2017), and generalized linear models (Rinne et al. 2018). All these methods, except for moving mean, have been used before for gap-filling CH_4 flux data from different mire ecosystems. The look-up table approach uses half-hourly data, while for the other three methods we used daily average data, as methane emissions from this ecosystem do not show diel cycle (See below, chapter 3.2).

The uncertainties due to each method were analyzed by the introduction of artificial gaps to the data, with lengths comparable to gaps existing in the year 2014. 35-day and 80-day gaps were implemented to the data of years 2015 and 2016. Gaps were placed in the winter period, to obtain similar gap distribution as in the year 2014 (gap distribution is presented below in Table 4). Annual sums, with artificial gaps, were compared with results from methods without those gaps. Statistical significances of differences between models were analyzed by using a two-sample t-Test for equal means with a 95 % confidence level (MATLAB R2019b).

2.6.1 REddyProc

The Jena gap-filling tool using look-up tables requires half-hourly data of CH_4 flux and environmental data: global radiation, air temperature, soil temperature, relative humidity, and friction velocity. Based on environmental data, fluxes are classified and averaged within a given time window. The missing data are then filled with the average value from classified data. Uncertainty can be estimated as standard deviations of fluxes within classes. Detailed information about the method is presented by Falge et al. (2001) and Wutzler et al. (2018).

2.6.2 Moving average

A 5-day moving mean approach is a very simple gap-filling method where the moving mean is calculated for subsets of the data. In case of a gap in the number of observations in the averaging window, the mean value is calculated for the fewer numbers of points. The method was applied on daily average CH_4 flux data using MATLAB (movmean function). For gaps longer than 5 days, linear interpolation was used between the last point before the gap and the first point after gap. Uncertainties of the single gap-filled flux were estimated by calculating the moving standard deviation (movstd function, MATLAB) on the same subset of the data like for the moving mean.

2.6.3 Artificial Neural Network

An artificial neural network (ANN) has been successfully applied for gap-filling of CH_4 fluxes by e.g. Dengel et al. (2013), Jammet et al. (2015,2017), and Knox et al. (2016). This type of ANN was designed in MATLAB using a fitnet function with 30 hidden neurons. We used the Levenberg-Marquardt algorithm as a training function (Levenberg 1944 Marquardt 1963). All available daily average CH_4 values were used to train (70 %), validate (15 %), or test (15 %) the ANN. The ANN requires input data without gaps to work properly and thus the short gaps (up to three days) in environmental daily averaged data were filled by linear interpolation before the ANN analysis. All environmental variables, except for the WTL were used as input for the ANN method. The WTL was excluded because it was not available during the frozen period, i.e. most of the year. The ANN method was applied to sectors and each year separately (ANN YbY) or all three years together. Multiple repetitions were done to minimize uncertainty connected with randomly chosen data points for training, validation, and testing. The network was trained and used to

https://doi.org/10.5194/bg-2021-81
Preprint. Discussion started: 6 April 2021

calculate the time series of CH_4 daily fluxes 100 times in each case of gap-filling. The number of repetitions was chosen to have a sample large enough to calculate reliable mean and standard deviation values, and to keep the computation time reasonably short. An average CH_4 flux for each day was calculated based on 100 daily values. The gaps in the measured flux time series were filled with values from the time series calculated by ANN. Errors were estimated as standard errors of mean on daily flux, based on 100 ANN trained values.

2.6.4 Generalized Linear Model

Generalized linear models (GLM) are linear combinations of linear and quadratic functions describing the dependence of response variables to predictors. In our case, the response variable was the logarithm of daily average CH_4 flux and predictors were daily averages of measured environmental variables. Controlling factors of CH_4 emission were examined by a procedure similar to the routine described by Rinne et al. (2018). A correlation matrix of linear correlation based on daily values of environmental factors and CH_4 fluxes was constructed (Figure S2). Additionally, the logarithm of CH_4 fluxes was added to the correlation matrix to check the exponential relationship between parameters. This type of relationship between CH_4 fluxes and peat temperature was previously found by e.g. Christensen et al. (2003), Jackowicz-Korczyński et al. (2010), Bansal et al. (2016), Pugh et al. (2017) and Rinne et al. (2018). Gap filled CO_2 flux, and gross primary production (GPP), were also included as prospective controlling factors. In order to avoid strong cross-correlation between predictors, first, we selected the parameter with the highest correlation and then removed parameters from the GLM development with a cross-correlation between parameters $R^2>0.6$. We thus chose GPP, soil temperature at 30 cm depth for the eastern sector and 10 cm depth for the western sector, soil water content (SWC), short-wave incoming radiation, and vapor pressure deficit (VPD) as possible predictors. The model was constructed in MATLAB using the stepwiseglm function (Dobson 2002). The GLM was made for both separately for each year (GLM YbY) or for all three years combined. Errors were estimated as 95 % confidence intervals because it was an output of the stepwise function. This method was also used for the determination of the controlling factors from the possible predictors.

2.7 Gap filling of CO_2 fluxes

CO_2 fluxes were calculated for the two sectors. CO_2 flux exhibited the diel pattern in the growing season, with uptake during daytime (Global radiation > 50 W m^{-2}) and release at night (Global radiation < 50 W m^{-2}). We used the ANN to gap-fill the time series of CO_2 fluxes. This method was chosen to check the possibility of reconstruction diel cycle. This diel pattern of CO_2 was taken into account by using half-hourly data. We used all environmental variables excluding the WTL, as for CH_4 fluxes. GPP was obtained by partitioning the gap-filled data using the Jena gap-filling tool. Finally, the half-hourly gap-filled GPP and CO_2 data were averaged to daily values.

https://doi.org/10.5194/bg-2021-81
Preprint. Discussion started: 6 April 2021

2.8 Contribution of palsa and thaw surfaces to average CH_4 emission

Using the average annual CH_4 emission from the two wind sectors and the relative contributions of the two surface types to the fluxes from these sectors we could calculate the average annual emission from these surface types. We could express the average annual CH_4 flux for the two sectors, F_e and F_w, with a pair of equations,

$$F_e = f_{e,p}E_p + f_{e,t}E_t, \quad (1)$$

$$F_w = f_{w,p}E_p + f_{w,t}E_t, \quad (2)$$

where f indicates the fractional contribution of surface type to the flux from the footprint calculations (subscripts e and w referring to east and west, respectively; and p and t to palsa and thaw surface, respectively) and E_p and E_t are emissions from palsa and thaw surface, respectively. We could solve this equation set with two unknowns to yield E_p and E_t.

2.9 Definition of seasons

The beginning of the unfrozen period was defined as the day when daily averages of peat temperature at 10 cm depth had been above 0°C for three consecutive days. The end of the unfrozen period was defined as the day when daily averages of peat temperature at 10 cm depth had been below 0°C for three consecutive days. The unfrozen and frozen periods commence in the western sector on average 3 days earlier than in the eastern sector, but differences in the unfrozen season length are not systematic (Table 1). The beginning and the end of the unfrozen season for both sectors were determined independently. The horizontal distance between soil temperature sensors in eastern and western sectors was around 75 m, differed about 2 m elevations, and were roughly 40 m from the flux tower.

Table 1. Start, end, and the length of the unfrozen periods in the footprints of the EC measurements.

	2014 W	***2015 W***	***2016 W***	***2014 E***	***2015 E***	***2016 E***
beginning of unfrozen period (DoY)	141	136	129	143	142	133
end of unfrozen period (DoY)	289	305	297	292	307	300
length of unfrozen season	148	169	168	149	165	167

https://doi.org/10.5194/bg-2021-81
Preprint. Discussion started: 6 April 2021

3 Results

3.1 Environmental conditions and flux footprints

Winds from eastern and western sectors contributed to 50 % and 40 % to the daytime wind directions, respectively (Figure 1). Northerly and southerly winds contributed to around 5 % each. In the nighttime, 51 % of wind was from the East and 32 % from the West. Additionally, 15 % of total wind came from the South during nighttime, probably as catabatic flow from higher mountain areas. The wind from North was rare, around 2 % of all the cases.

The annual average peat temperature of the uppermost 50 cm of peat was systematically warmer in the eastern sector than in the western sector (Table 2; Figure 2). However, the summertime peat temperature at the top 10 cm layer was warmer for the western sector (Figure S3). The situation was the opposite during winter when the western sector down to 50 cm was colder than the eastern sector. The western sector, was colder than the eastern sector, causing the existence of permafrost. Temperature differences, between both areas, at the same depth, were stable over the measurement years. The biggest difference was noticed at a depth of 30 cm. The temperature at 30 cm and 50 cm depth was increasing during consecutive years.

Figure 2. Time series of daily mean values for western and eastern sectors for: peat temperature (top panel), soil moisture (middle panel), and water table level (bottom panel), where the shaded light blue area is frozen period, when peat temperature at 10 cm was below 0^0C (see chapter 2.8 for detailed description).

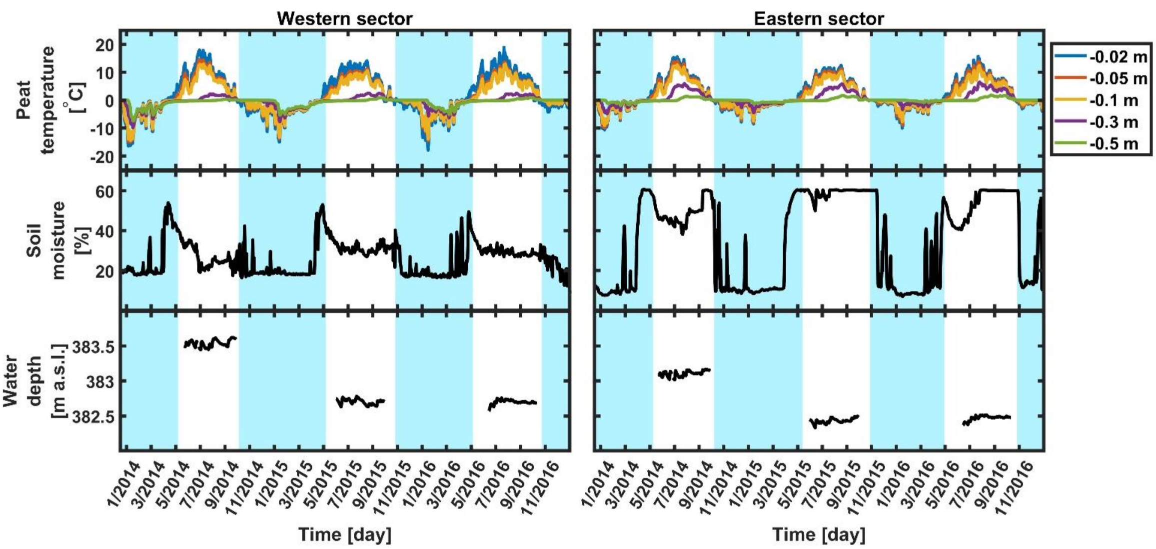

https://doi.org/10.5194/bg-2021-81
Preprint. Discussion started: 6 April 2021

Table 2. Mean annual peat and air temperature for the years 2014-2016 for eastern and western sectors.

Temperature [^{0}C]									
depth in cm	***2014 E***	***2014 W***	***2014 E-W difference***	***2015 E***	***2015 W***	***2015 E-W difference***	***2016 E***	***2016 W***	***2016 E-W difference***
ambient air	0.30		-	0.14		-	0.35		-
2	1.62	1.38	0.24	2.21	1.96	0.25	2.17	1.93	0.24
5	1.37	0.84	0.53	1.95	1.29	0.65	1.93	1.29	0.64
10	1.19	0.54	0.64	1.70	1.05	0.65	1.70	1.10	0.60
30	0.34	-0.88	1.21	0.61	-0.58	1.19	0.82	-0.48	1.30
50	-0.12	-0.97	0.85	-0.04	-0.79	0.75	0.16	-0.65	0.80

The WTL was higher in 2014 than in 2015 and 2016 according to measurements both in the eastern and western sectors (Figure 2). This is not reflected in the SWC measurements, which is probably due to the different locations of the measurements of WTL and SWC. In the western sector the WTL was measured in an isolated wet patch, surrounded by drier palsa and thus it is not representative of the dominating type of this area. The WTL in the eastern sector was more representative of the area of the footprint. Data from the WTL probe in the West part of the mire was excluded from the further analysis as it does not represent the situation for the majority of the western sector. The soil moisture was higher for the eastern than the western sector during all years. The data shows a distinctive step change at thaw and freeze, as the dielectricity of ice and liquid water differ. In the eastern sector, the soil was fully saturated for most of the unfrozen period during the years 2015-2016, while 2014 indicates lower water content levels. The western sector was not fully saturated at any time during the years 2014-2016.

Footprint and flux contribution of drier and wetter areas are presented in Figure 3. The dry areas (yellow) contribute to more than 90 % fluxes from the western sector. In the eastern sector, the wetter (blue) and drier areas contribute almost equally to the fluxes. The contributions of the wet and dry areas to the fluxes in both sectors were stable across the three study years.

Figure 3. Footprint climatology for westerly and easterly wind at the SE-Sto tower (upper panel) for the year 2014 and relative amounts of wetter areas (blue) and drained palsa area (yellow) inside the 80 % area of influence of the footprints. The black cross is the location of the tower and each red line indicates 10 % of the contribution from the source area to measured fluxes at the tower. The footprint climatology is almost identical for all study years, see bottom panel.

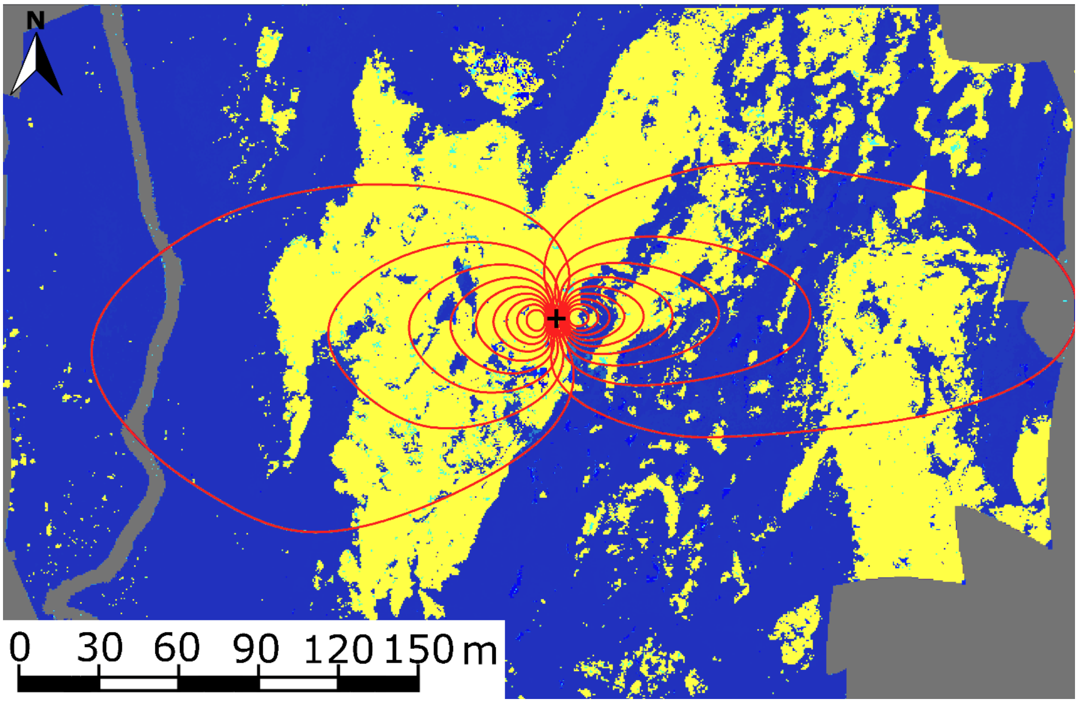

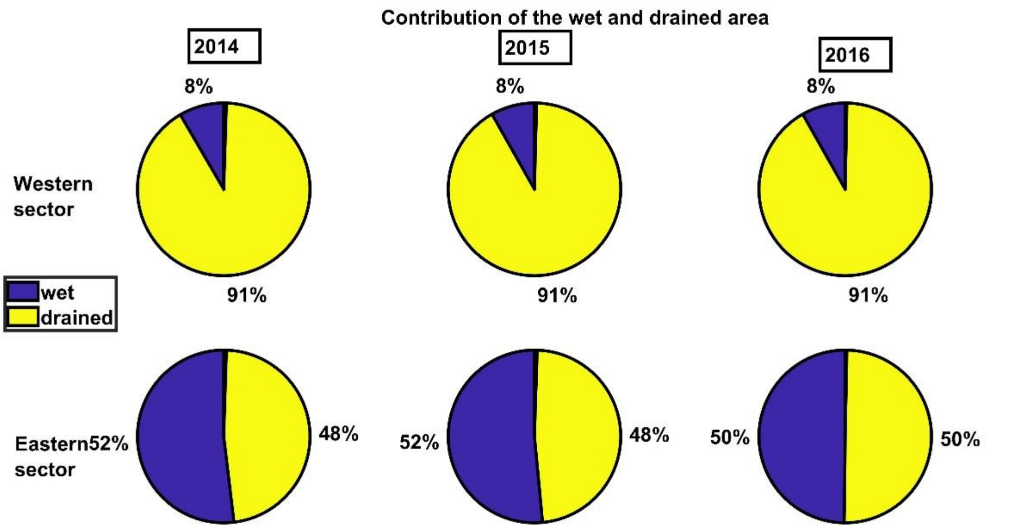

3.2 CH_4 fluxes

The possible diel cycle of CH_4 fluxes was analyzed during the growing season of each year and both wind sectors separately. This was done by normalizing each half-hourly flux by dividing it

https://doi.org/10.5194/bg-2021-81
Preprint. Discussion started: 6 April 2021

with the daily median from that day and then calculating the median normalized flux for each half-an-hour period of the day for the whole growing season (Rinne et al. 2007). This yielded a normalized diel cycle of CH_4 fluxes. As seen in Figure S4, no diel cycle was observed. Thus, it is possible to calculate CH_4 daily averages without gap-filling the diel cycle, similarly to e.g. Rinne et al., (2007, 2018) and Jackowicz-Korczyński et al. (2010). We discarded daily averages with less than 10 flux data points from further analysis, to ensure the reliability of the daily average fluxes. Uncertainties of daily averages were calculated as standard errors of the mean. The size of the available flux data set, after averaging, is presented in Table 3. The gap distribution in the datasets for the different sectors and years is presented in Table 4.

Table 3. The size of available daily data sets after averages for each year and wind sector.

	2014 E	***2015 E***	***2016 E***	***2014 W***	***2015 W***	***2016 W***
total number of points	*365*	*365*	*366*	*365*	*365*	*366*
number of points after averaging	*137*	*174*	*182*	*96*	*167*	*178*
% of available data	*38*	*48*	*50*	*26*	*46*	*49*
% of available data during winter period	*36*	*54*	*56*	*12*	*36*	*37*
% of available data during unfrozen period	*40*	*41*	*42*	*47*	*58*	*63*

Table 4. Gaps distribution over years and wind direction.

Type of gap	***Length of gap***	***2014 E***	***2015 E***	***2016 E***	***2014 W***	***2015 W***	***2016 W***
short gap	***1-3 day***	*32*	*50*	*41*	*24*	*44*	*36*
medium gap	***4-7 day***	*7*	*12*	*11*	*6*	*8*	*11*
long gap	***8-30 day***	*3*	*7*	*4*	*4*	*6*	*6*
very long gap	***> 30 day***	*1*	*0*	*0*	*3*	*0*	*0*

Daily non-gap-filled CH_4 fluxes showed a characteristic annual cycle, with peak emissions in August (Figure 4) and low but positive wintertime fluxes. These fluxes were statistically different from zero ($p<0.001$, two-sided Wilcoxon rank sum test). Winter fluxes from the western and eastern sectors were also different from each other ($p<0.001$).

CH_4 fluxes, both from the western sector and the eastern sector started increasing after snowmelt up to the maximum in August (Figure 4). No major springtime emission burst nor autumn freeze-in burst were observed in any of the years.

https://doi.org/10.5194/bg-2021-81
Preprint. Discussion started: 6 April 2021

Figure 4. Time series for non-gap-filled CH_4 daily averaged fluxes for the western sector (green triangles) and the eastern sector (black dots), where the shaded light blue area is frozen period when peat temperature at 10 cm was below 0^0C (see chapter 2.8 for detailed description).

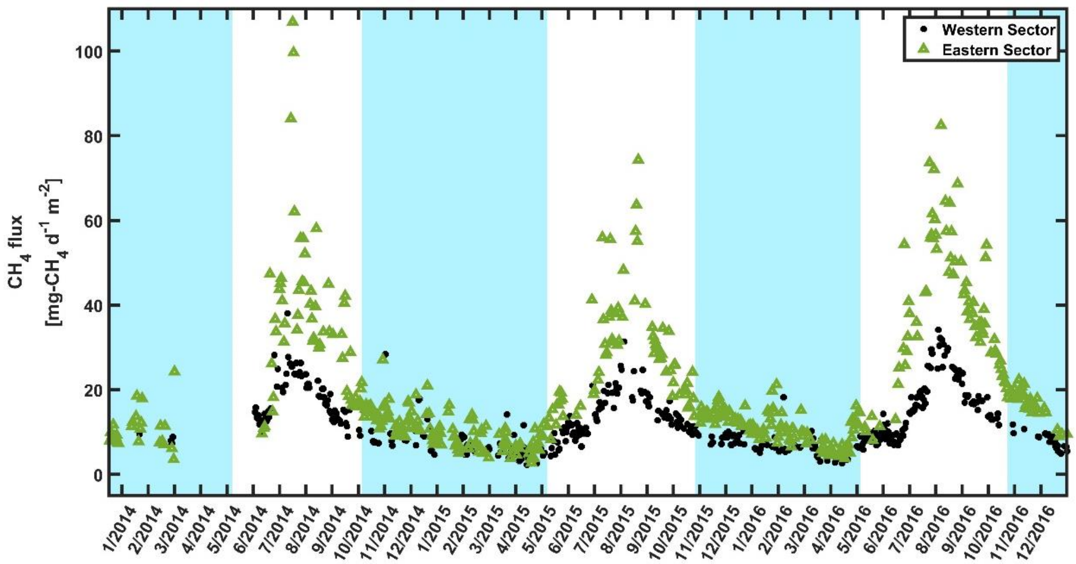

The peak season of the CH_4 emission was defined as two weeks forward and backward from the day with the maximum daily emission in a given year. The average emission during the peak seasons was 56 mg-CH_4 m^{-2} d^{-1} for the eastern thawing wet sector and 24 mg-CH_4 m^{-2} d^{-1} for the western sector. Detailed emissions for all years are presented in Table 5. The peak season emissions were statistically different from each other ($p<0.001$). Wintertime fluxes were steadily declining as winter continued and the lowest emissions were observed slightly before the spring thaw. Wintertime average emissions were 24 mg-CH_4 m^{-2} d^{-1} for the eastern sector and 16 mg-CH_4 m^{-2} d^{-1} for the western sector. Detailed emission of winter periods is presented in Table 6.

Table 5. CH_4 emission during the peak season

	Mean	*Standard deviation*	*The standard error of the mean*
	[mg-CH_4 m^{-2} d^{-1}]		
2014 E	54.2	22.3	6.5
2015 E	55.3	13.2	2.8
2016 E	59.9	9.4	2.7
2014 W	22.6	4.5	1.2
2015 W	21.4	4.2	1.1
2016 W	28.2	3.7	1

https://doi.org/10.5194/bg-2021-81
Preprint. Discussion started: 6 April 2021

Table 6. CH_4 emission during the winter period

	Mean	***Standard deviation***	***The standard error of the mean***
	[mg-CH_4 m^{-2} d^{-1}]		
2014 E	24.1	5.5	0.7
2015 E	22.3	3.5	0.4
2016 E	26.3	5	0.5
2014 W	19.2	5.2	1.1
2015 W	14.9	2.8	0.4
2016 W	14.0	3.1	0.4

3.3 Factors controlling the CH_4 fluxes

In the eastern sector, the CH_4 flux correlated best with the peat temperature at 30 cm depth, and in the western sector with the temperature at 10 cm depth. Using temperatures above the level of maximum correlation led to similar hysteresis-like behavior in CH4 flux - temperature relations as presented by Chang et al., (2020), but using deeper temperatures led to inverse hysteresis compared to shallower temperatures (Figure 5). The correlation matrix (Figure S2) shows the importance of SWC in the CH_4 emissions, while WTL does not correlate significantly with CH_4 flux. Controlling factors were examined before and after temperature normalization (Table 7), to avoid effect of cross-correlation between explanatory parameters.

Figure 5. Weekly averages of CH4 fluxes vs surface peat temperature (top panels), vs the best correlated layer (middle panels), and vs the deeper layer (bottom panel). Data were divided into the beginning of the growing season (blue dots) and end of the growing season (orange triangles), where breakout week was the week with the highest emission.

https://doi.org/10.5194/bg-2021-81
Preprint. Discussion started: 6 April 2021

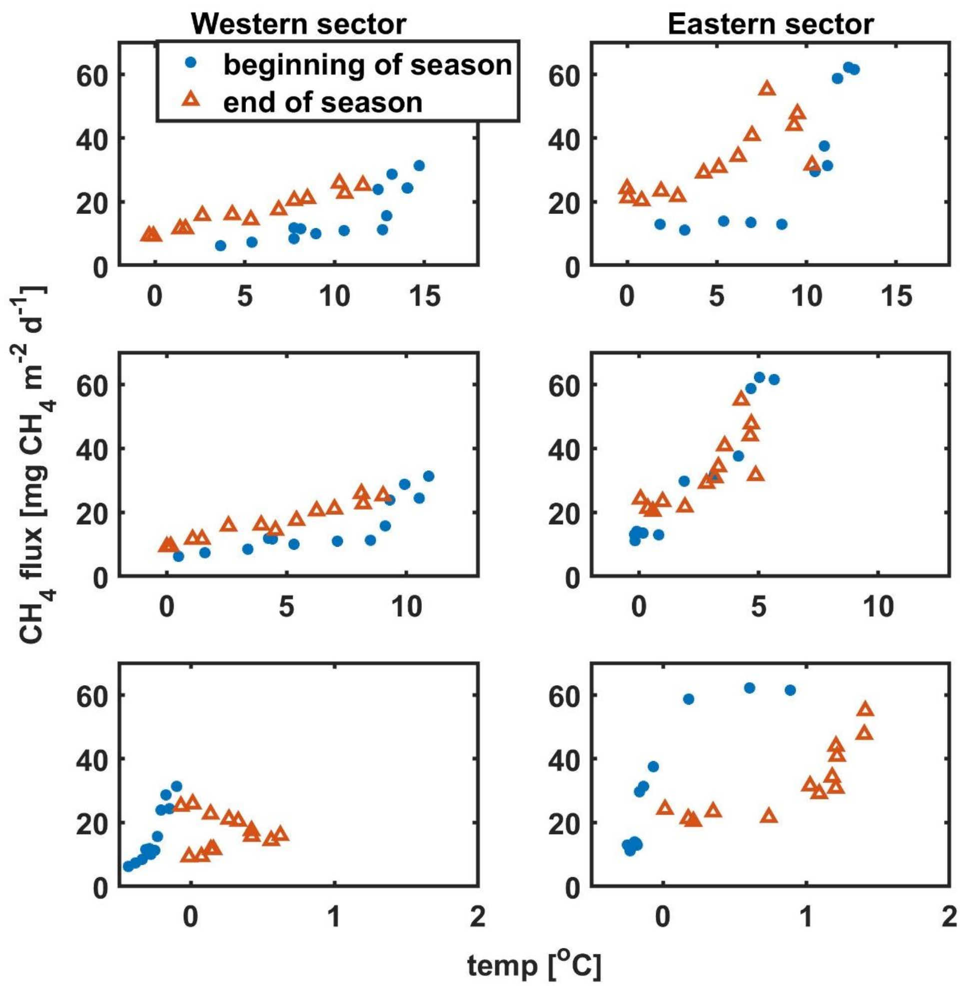

The result from GLM, showing the variables that contribute to the model, is presented in Table S2. The parameter which was selected first by all models, was peat temperature, at 10 cm depth for the western sector and at 30 cm depth for the eastern sector. For the eastern sector, the GLM algorithm selected SWC as the explanatory factor for CH_4 fluxes during all years as well as for the combined three-year period. The GLMs created for the western sector did not have other explanatory factors besides the peat temperature that were selected in all years. However, two more explanatory factors, GPP and shortwave incoming radiation, appeared in the three time periods (years 2015 and 2016, and three-years combined) for the western sector.

https://doi.org/10.5194/bg-2021-81
Preprint. Discussion started: 6 April 2021

The eastern sector models had shortwave incoming radiation as the explanatory factor for the year 2015, the year 2016, and combined three-year period. A unique variable for this sector was the vapor pressure deficit, which was used in the models constructed for the years 2016 and combined three-year period.

The year 2014 for both sectors was characterized by a smaller number of parameters contributing to the models for both sectors compared to other years and combined three-year models. Only peat temperature and SWC were explanatory variables for both sectors in this year. The years 2015 and 2016 and all three years combined have a longer list of parameters.

As the WTL data was available only during a short period of the year, it was not analyzed with usage of the GLM. The WTL measurement in the western sector was not representative of the conditions for most of the sector, this parameter was not used for further analysis from this sector. The WTL was correlated with CH_4 fluxes for the eastern sector.

Based on the chosen explanatory variables it could be noticed that the seasonal cycle could be explained a lower number of parameters than the interannual variation.

Table 7. Summary of controlling factors before and after temperature normalization

Year and ecosystem	***R for CH_4 flux***	***the p-value for CH_4 flux***	***R for temperature normalized CH_4 flux***	***the p-value for temperature normalized CH_4 flux***
		GPP		
2014 E	0.71	$7x10^{-22}$	-0.03	0.70
2015 E	0.69	$2x10^{-25}$	0.02	0.83
2016 E	0.77	$1x10^{-36}$	0.21	$4x10^{-3}$
2014 W	0.69	$4x10^{-15}$	-0.10	0.36
2015 W	0.73	$6x10^{-29}$	0.05	0.56
2016 W	0.71	$5x10^{-29}$	-0.02	0.76
		WTL		
2014 E	-0.48	$2x10^{-4}$	$-6x10^{-3}$	0.96
2015 E	-0.16	0.3	-0.2	0.18
2016 E	0.57	$4x10^{-6}$	-0.33	0.01
		SWC		
2014 E	0.51	$2x10^{-10}$	-0.02	0.79
2015 E	0.51	$1x10^{-12}$	-0.03	0.66
2016 E	0.69	$1x10^{-26}$	0.2	$6x10^{-3}$
2014 W	-0.31	$2x10^{-3}$	-0.37	$2x10^{-4}$
2015 W	0.19	0.02	-0.19	0.02
2016 W	0.22	$3x10^{-3}$	-0.26	$5x10^{-4}$

https://doi.org/10.5194/bg-2021-81
Preprint. Discussion started: 6 April 2021

3.4 Gap-filled annual cycles

Cumulative CH_4 emissions based on different gap-filling methods are presented in Figure 6. All follow a similar annual curve, with a steeper increase in summer, but also relatively high wintertime contribution. Annual, wintertime, and unfrozen period emissions by all gap-filling methods, with their estimated uncertainties, are shown in Figure 7. Emission estimation by each sector and data gap-filled by the different method are presented in Table S3. Average values from all models with their upper and lower limit and wintertime contribution to fluxes are demonstrated in Table 8.

Figure 6. The cumulative sum of CH_4 fluxes for the years 2014-2016 for western and eastern sectors calculated with the different gap-filling methods. ANN - the artificial neural network for all years, ANN YbY - artificial neural network each year separately, Jena - Jena online gap-filling tool, MM - moving mean with 5-day moving window, GLM- the general linear model for all years, GLM YbY - the general linear model for each year separately. The shaded light blue area is frozen period when peat temperature at 10 cm was below 0^{0}C (see chapter 2.8 for detailed description).

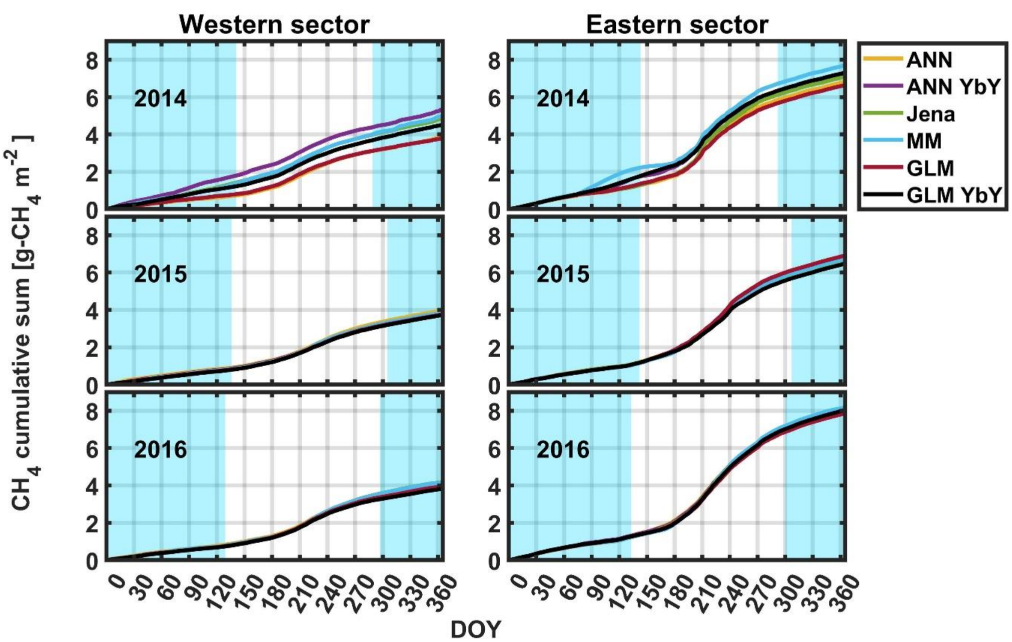

Figure 7. Comparison of cumulative sums of CH_4 fluxes for different gap-filling methods for the western sector (top panel) and eastern sector (bottom panel). ANN - the artificial neural network for all years, ANN

https://doi.org/10.5194/bg-2021-81
Preprint. Discussion started: 6 April 2021

YbY - artificial neural network each year separately, Jena - Jena online gap-filling tool, MM - moving mean with 5-day moving window, GLM- the general linear model for all years, GLM YbY - the general linear model for each year separately. Gray bars are for the annual sums, blue bars are for the frozen period sums and green bars are for the unfrozen period (see chapter 2.8). Solid lines are the mean value from all models and dashed lines are for the standard deviation range, with the same colors described above.

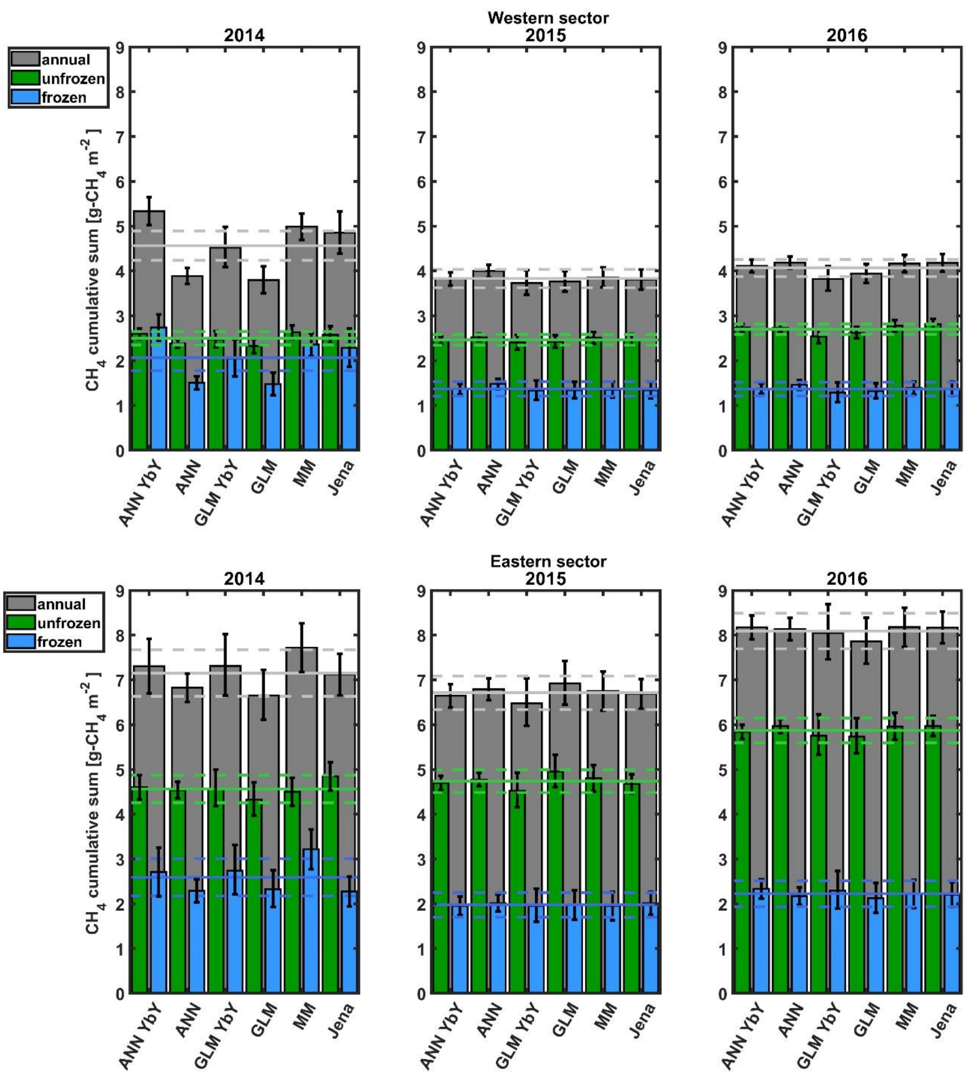

As seen in Table 4, the year 2014, with a larger difference between annual emissions calculated by different gap-filling methods, had very long gaps that were not present in other years. Also, the uncertainties in annual emission are the largest for the year 2014 for all gap-filling methods, reflecting the gap distribution.

https://doi.org/10.5194/bg-2021-81
Preprint. Discussion started: 6 April 2021

Table 8. Average CH_4 annuals emission based on all models with the upper and lower limit and contribution to the winter fluxes.

	Mean	***Lower limit***	***Upper limit***	***Contribution to wintertime fluxes***	***Mean***	***Lower limit***	***Upper limit***	***Contribution to wintertime fluxes***
	Western sector				***Eastern sector***			
	g-CH_4 m^{-2} yr^{-1}			***%***	***g-CH_4 m^{-2} yr^{-1}***			***%***
2014	4.6	3.8	5.3	45	7.2	6.7	7.7	36
2015	3.8	3.7	4	36	6.7	6.5	6.9	29
2016	4.1	3.8	4.2	34	8.1	7.9	8.2	27

Three years' averages of GPP and net ecosystem exchange (NEE) for two sectors are presented in table 9. As a comparison, data from a tall sedge fen area, where permafrost was completely thawed, of Stordalen Mire by Jammet et al. (2017) are presented, showing that the fen has the highest percentage of carbon emitted as CH_4. The eastern and the western sectors emitted less of the carbon as CH_4.

Table 9. Average annual GPP, NEE and CH_4 emission from western and eastern sector in comparison to fen.

	GPP	**NEE**	**CH_4**	**CH4/GPP**	**CH4/NEE**
	g-C m^{-2}	**g-C m^{-2}**	**g-C m^{-2}**	**%**	**%**
Western sector	225	-28.9	3.1	1.4	19.6
Eastern Sector	257	-42.0	5.5	2.2	14.0
Fen (Jammet et al. 2017)	N.A.	-66.3	21.2	N.A.	32.0

The average annual CH_4 emissions of palsa and thawing surfaces, as calculated by Eqs. (1) and (2), are presented in Table 10. For comparison average annual emissions from other major surface types, measured by EC technique, are shown as well. The emission from the tall graminoid fen, a third mire type common at Stordalen Mire, has been previously measured using the EC method by Jackowicz-Korczyński et al. (2010) and Jammet et al. (2017). In addition to these, the mire complex includes shallow lakes. Their annual CH_4 emission has been measured by EC method by Jammet et al., (2017).

Table 10. Annual CH_4 emission from different components of the Stordalen Mire complex from EC studies.

https://doi.org/10.5194/bg-2021-81
Preprint. Discussion started: 6 April 2021

type of wetland	*Annual emission [g-CH_4 m^{-2} yr^{-1}]*	*References*
palsa plateau surface	3.6 ± 0.7	this study
thawing wet surface	11 ± 2	this study
thawed fen	21.1 ± 2.2	Jackowicz-Korczyński et al. 2010
	28.3 ± 1.7	Jammet et al. 2017
shallow lake	6.5 ± 0.8	Jammet et al. 2017

4 Discussion

4.1 Differences in controlling factors

According to the GLM, peat temperature and GPP were typically the first parameters selected by the algorithm to explain CH_4 fluxes. In the eastern sector, the CH_4 flux correlated best with the peat temperature at 30 cm depth, and in the western sector with the peat temperature at 10 cm depth. Temperature as a controlling factor of CH_4 emission has been reported in many wetlands studies (Christensen et al. 2003, Jackowicz-Korczyński et al. 2010, Bansal et al. 2016, Pugh et al. 2017, Rinne et al. 2007; 2018), in line with our findings. The correlation of CH_4 fluxes with the temperature at 5 cm depth was also higher than for 30 cm in the western sector. As the peat in the palsa is frozen at 30 cm depth for most of the growing season, the correlation between CH_4 fluxes and temperature at these depths is lower. Temperature correlation for the upper part, 2 cm, and 5 cm depth, shows a similar level of correlation as presented by Jackowicz-Korczyński et al. (2010). As they did not analyze correlation with the temperature at deeper peat, we cannot compare these results. The hysteresis-like behavior of the CH_4 flux – temperature relation is similar to that observed by Chang et al. (2020) when using temperatures measured above the depth of maximum correlation, but inversed when using temperatures measured at deeper depths (Figure 5). This is in line with at least part of the hysteresis-like behavior to be due to the lag of seasonal temperature wave at the depth of methane production compared to the timing of the temperature wave at shallower depth or air temperature.

GPP was indicated as a controlling factor for CH_4 emission from a boreal fen ecosystem by Rinne et al. (2018). In our study, the correlation matrix shows a significant correlation between daily average GPP and CH_4 flux at both sectors (Table S3). To disentangle the confounding effects of temperature and GPP, we used temperature-normalized CH_4 fluxes following Rinne et al. (2018) which revealed that the correlation between GPP and temperature-normalized CH_4 flux was not significant in most years, Table 7. Only the data from the eastern sector in the year 2016 shows a significant correlation. Thus, it seems hard to disentangle the effects of temperature and GPP on CH_4 fluxes using this data set. As our data set consists of only three years, the analysis of interannual variations would not be a robust approach either.

Solar shortwave radiation was selected as a controlling variable by 6 of 8 GLM models (Table S3). This parameter has an indirect effect on CH_4 production via photosynthesis and subsequent substrate production. The maximum emission of CH_4 occurs later in the year than maximum radiation. This may be due to the CH_4 emission depending on the deeper peat temperature or

https://doi.org/10.5194/bg-2021-81
Preprint. Discussion started: 6 April 2021

seasonal cycle of available substrates, lagging behind the annual cycle of radiation (e.g. Rinne et al., 2018; Chang et al., 2020). The highest correlation of CH_4 flux and radiation was observed in 2014, but GLM did not select radiation as an explanatory factor for this year. Other years and the whole period show a much lower correlation.

CH_4 fluxes from wetlands have been shown to depend on WTL in many studies (e.g. Bubier et al., 2005; Turetsky et al., 2014; Rinne et al., 2020). However, in a number of studies, the CH_4 fluxes have shown to be relatively insensitive to the small variation, without strong extreme conditions, in the WTL (Rinne et al. 2007, 2018, Jackowicz-Korczyński et al. 2010). In the eastern sector, CH_4 flux and WTL were correlated for the years 2014 and 2016. However, after normalization of CH_4 fluxes with their temperature dependence following Rinne et al., (2007), correlations were mostly not significant (Table 7). This is similar to conclusions drawn by e.g. Rinne et al. (2007, 2018) and Jackowicz-Korczyński et al. (2010).

Instead of WTL, we used SWC as a possible controlling factor for the CH_4 emission from the western sector. Sturtevant et al. (2012) also reported SWC as a controlling factor in autumn. SWC shows correlation on a significant level before and after normalization for three years for the western sectors (Table 7).

The GLM algorithm selected SWC as one of the explaining factors while constructing the GLM for the eastern sector for the whole measurement season. It was chosen by models built for three years together and each year separately. R and p-value are presented in Table 7. A reduction of R and increase in p-value after temperature normalization is similar to previous parameters. The correlation of CH_4 emission with SWC stays on a significant level only in the year 2016.

4.2 Gap-filling methods

In general, the gap-filled annual CH_4 emissions were within their estimated uncertainty from each other, apart from the year 2014. The results of different gap-filling methods were affected by the different gap distributions and lengths in different years and the two wind sectors. Thus, below we discuss the method performance separately for the year 2014 and the two other years.

The dataset from the eastern sector was gap-filled with less uncertainty than for the western sector in 2014. The data from the eastern sector contains fewer very long gaps - more than 30 days, and fewer long gaps - more than 8 but less than 30 days. The method which was most affected by long gaps was the moving mean approach, indicating that this method should not be used for data sets with very long gaps. The ANN and the GLM gap-filling methods based on the whole data set estimated lower annual emission than mean emission from all methods. For two years without very long gaps (2015 and 2016), the Jena gap-filling tool was assumed as a baseline method, as it is commonly used for gap-filling of especially CO_2 fluxes. It is independent of the user choices, as the ecosystem variables required have been chosen by the developers. However, as this gap-filling tool has been developed with CO_2 in mind, not all the variables are necessarily

https://doi.org/10.5194/bg-2021-81
Preprint. Discussion started: 6 April 2021

relevant for the gap-filling of the CH_4 time series. Furthermore, the Jena gap-filling tool works in a half-hourly resolution to resolve the diel variation in CO_2 fluxes. As the sub-daily variation in CH_4 fluxes is largely random noise in many mires (Rinne et al., 2007; 2018; Jackowicz-Korczyński et al., 2010), developing a similar tool working at daily time step for CH_4, and with tailored parameter set for methane, would be useful.

The moving mean approach resulted in annual fluxes within the range of standard deviation from the Jena gap-filling tool. Daily values could vary less than values obtained by the Jena tool because moving means smooth the data. Additional advantages of this method are low requirements, as no auxiliary data is needed.

Annual estimates of CH_4 emission, based on the gap-filling with algorithms developed for the whole data set, could be biased when the ecosystem is changing fast between the years and functional dependencies on environmental parameters change. The annual CH_4 emissions by ANN, based on the whole data set and based on one-year data, agree within the standard deviation for the years 2015 and 2016. Both of them are als oin agreement with the baseline method within the standard deviation.

The feasibility of GLM is similar to ANN. The GLM model built on the whole dataset is sensitive to rapid changes in ecosystem functioning and the number of gaps each year. A year with more gaps has a lower influence on the model, similarly to the ANN. However, annual CH4 emissions derived using GLMs, based on each year separately or the whole dataset, agree with one another and with baseline model within the standard deviation. GLM required more preparation than ANN. Before developing the GLMs, highly correlated parameters need to be determined. The selection of relevant variables is crucial for the correct performance of that algorithm and the selection influences model output and model uncertainties.

According to the analysis with artificial gaps, the 35-day artificial gap did not change annual sums significantly for any gap-filling method. The 80-day artificial gap created a significant difference for the eastern sector in the year 2015 for ANN YbY and 2016 for ANN, Figure S5. The unfrozen period did not show significant differences between annual sums for any method. The wintertime period was statistically different for the year 2015 for ANN YbY. The results with the 80-day gap had higher uncertainties than the results with a 35-day gap. The existence of gaps in the winter period did not have a significant impact on the unfrozen period fluxes.

All presented methods show similar emissions. Choosing one of them as the most appropriate is not obvious, because all of them has strong and week points. Method required the less preparation before use, so the faster to apply is moving mean. It can be used for the short gaps with the good results and does not need additional measured variables to work properly. The ANN method require less preparation than other methods i.e. following the template or choosing the correct variables and it gives similar results. It could be recommended as a gap-filling method suitable for different sites due to unique construction of the ANN for each place.

4.3 Winter fluxes

The winter fluxes from both sectors were positive, which is in line with observations by e.g. Rinne et al. (2007, 2018, 2020) and Jammet et al. (2017) of wintertime CH_4 emissions from frozen northern mires. Winter emission and potential spring thaw bursts of CH_4 can be mechanistically connected (Taylor et al. 2018), while degassing of CH_4 during the winter is likely to lead to smaller or no thaw bursts of CH_4. Thus, EC studies on the seasonal cycle of CH_4 emissions from other seasonally frozen mire ecosystems have shown minor or no thaw emission pulse (Rinne et al., 2007; 2018; Mikhaylov et al. 2015). On the contrary, many studies show spring-thaw emissions from shallow lakes (Raz-Yaseef et al. 2017, Jammet et al. 2015, 2017). In lakes, winter fluxes can be blocked by a solid ice layer leading to the build-up of CH_4 below ice during the frozen period (Jammet et al. 2017). On mires, however, the ice cover is not as solid as in lakes, but more porous due to peat and plants within the ice. Therefore, the diffusion during the frozen period is considerably faster than through lake ice. Furthermore, Song et al. (2012) showed that spring burst events could occur at a very small scale and very short in duration (e.g. 2 hours). Small-scale events show a lower influence on EC measurements because the method averages over a larger area. Moreover, if the small-scale short-duration event does not happen in the EC footprint e.g. due to wind direction, it will be missed.

We did not observe an autumn freeze-in burst in our data from either sector at Stordalen Mire. These events have been observed at a High-Arctic tundra site (Mastepanov et al. 2013) though not every year. Mastepanov et al. (2008) suggested that freeze-in bursts of CH_4 could be observed only in the Arctic with continuous permafrost and not in a subarctic area with discontinuous or sporadic permafrost. The phenomenon is assumed to be connected to the expansion of water upon freezing, causing air bubbles to be mechanically pushed out of the freezing soil.

4.4 Different permafrost status and CH_4 emissions

Stordalen Mire is a complex mire system, with at least three different main wetlands surface types and different permafrost statuses within a distance of a few hundred meters. The permafrost palsa development and thaw depend both on temperature and snow cover and it is partly self-regulating via the effect of microtopography on local snow depth (Johansson et al. 2006). Due to the recently increasing temperatures, the thaw processes are currently likely to dominate over palsa growth. CH_4 emission from the different microforms in mire systems depends on a hydrological and nutrient status and temperature which affect e.g. plant and microbial communities.

The carbon emitted as the CH_4 fluxes from the eastern and western sector is on similar level to the Siikaneva fen (Rinne et al. 2018). In comparison to the other fens sites reviewed by Rinne et al. 2018, ratio of CH_4 to NEE at Stordalen Mire is higher. The reason behind this could be shorter growing season and thus lower CO_2 fluxes.

https://doi.org/10.5194/bg-2021-81
Preprint. Discussion started: 6 April 2021

The average annual CH4 emissions from different surfaces (Table 10) shows that the palsas have the lowest annual CH_4 emission, followed by a lake. The fully thawed fen, dominated by tall graminoids, has very high annual CH_4 emission and the highest of the mire complex, surpassing e.g. many boreal poor fens (Nilsson et al., 2008; Rinne et al., 2018). The thawing surfaces common in the eastern footprint have annual CH_4 emission between palsas and tall sedge fen. The three surface types studied here and previously by Jackowicz-Korczyński et al. (2010) and Jammet et al., (2017) can be seen as forming a thaw gradient in this subarctic environment. The globally rising temperature is likely to lead to continuing permafrost thaw in this kind of system and increased CH_4 emissions.

5 Conclusion

At our study site, eddy covariance fluxes were measured for two different subarctic mire areas, one dominated by palsa plateaus and the other a mixture of palsas and thawing wet surfaces. The measurements revealed clear differences in their annual CH_4 emission, with the area dominated by palsas emitting less. The annual emission from thawing surface (11 g-CH_4 m^{-2} d^{-1}) was nearly three times higher than from palsa surfaces (3.6 g-CH_4 m^{-2} d^{-1}) but only half of the emission previously reported from fully thawed tall graminoid fen. Areas measured in this study had similar seasonal cycles of emission, with maxima appearing in August and lower but significant fluxes in winter. The seasonal cycles were furthermore characterized by a gentle increase in spring and a more rapid decrease in fall, without any obvious burst events during spring thaw or autumn freeze-in. The wintertime period contributed with 27-45 % to the annual emission.

According to the correlation matrix and GLM analysis, CH_4 emissions from the western and eastern sectors were partly controlled by different factors. As in most studies on CH_4 emission from wetlands, peat temperature was the most important factor explaining the emission. However, the temperature at different depths seemed to control the CH_4 fluxes for the two analyzed mire sectors. The relation of CH_4 flux with peat temperature at shallower depths showed similar hysteresis-like behavior than observed by Chang et al. (2020), but inverse behavior with temperature at deeper peat.

The correlation of CH_4 emission and WTL in the eastern sector was not significant, but in the western sector, the SWC did appear to control the emission.

The estimation of annual CH_4 emission was based on gap-filling with four different methods. All methods resulted in rather similar annual fluxes, especially for the two years with just relatively short gaps. The performance of methods was dependent on a gap distribution. The longer gaps were the most problematic to be reconstructed by any of the methods. The average annual emission from the western sector was 4.2 g-CH_4 m^{-2} yr^{-1} and from the eastern sector was 7.3 g-

CH_4 $m^{-2}yr^{-1}$. Both were substantially lower than those obtained from a tall graminoid fen at the same mire system.

Based on the presented results further studies should focus on winter fluxes, which are important in the northern, low emissions wetlands with discontinuous permafrost. There is still a lack in understanding of the processes behind those emissions. Also, the origin of wintertime CH_4 emission is somewhat unknown. On the one hand, CH_4 can be produced during the winter period, on the other hand CH_4 can also be produced during the growing season, remain stored in the peat and then be slowly released during the frozen period. These processes could possibly explain the hysteresis-like behavior of CH_4 emissions.

Data and code availability

http://doi.org/10.5281/zenodo.4640164s

Author contribution

P.Ł., J.H. T.F., P.C. and J.R. analysed and interpreted the data. P.Ł., J.H., P.C., J.R. wrote the manuscript. T.F., P.C. and, N.R. designed the measurements. N.K. was responsible for the footprint calculation and its interpretation. P.-O.O. and L.E. were responsible for interpreting UAV data.

Competing interests

The authors declare that they have no conflict of interest

Acknowledgements

This study is funded by MEthane goes Mobile: MEasurement and MOdeling (MEMO2) project from the European Union's Horizon 2020 research and innovation programme under the Marie Sklodowska-Curie grant agreement No 722479. Data was provided by the Abisko Scientific Research Station (ANS) and Swedish Infrastructure for Ecosystem Sciences (SITES, co-financed by the Swedish Research Council) hosting the Stordalen site, part of the ICOS-Sweden network which was co-financed by the Swedish Research Council (grant-no. 2015-06020, 2019-00205). Image collection using the UAV was done by Matthias Siewert in collaboration with the SITES Spectral project.

References

Aubinet, M., Vesala, T., & Papale, D. (Eds.) (2012). Eddy covariance—A practical guide to

https://doi.org/10.5194/bg-2021-81
Preprint. Discussion started: 6 April 2021

Biogeosciences Discussions

measurement and data analysis. Dordrecht: Springer. 978-94-007-2350-4

Bubier, J., Moore, T., Savage, K., & Crill, P. (2005). A comparison of methane flux in a boreal landscape between a dry and a wet year. *Global Biogeochemical Cycles*, *19*(1). https://doi.org/10.1029/2004GB002351

Callaghan, T. V, Bergholm, F., Christensen, T. R., Jonasson, C., Kokfelt, U., & Johansson, M. (2010). A new climate era in the sub-Arctic: Accelerating climate changes and multiple impacts. *Geophysical Research Letters*, *37*(14). https://doi.org/10.1029/2009GL042064

Callaghan, T. V, Jonasson, C., Thierfelder, T., Yang, Z., Hedenås, H., Johansson, M., … Sloan, V. L. (2013). Ecosystem change and stability over multiple decades in the Swedish subarctic: complex processes and multiple drivers. *Philosophical Transactions of the Royal Society B: Biological Sciences*, *368*(1624), 20120488. https://doi.org/10.1098/rstb.2012.0488

Chang, K.-Y., Riley, W. J., Crill, P. M., Grant, R. F., & Saleska, S. R. (2020). Hysteretic temperature sensitivity of wetland CH4 fluxes explained by substrate availability and microbial activity. *Biogeosciences*, *17*(22), 5849–5860. https://doi.org/10.5194/bg-17-5849-2020

Christensen, T R, Friborg, T., Sommerkorn, M., Kaplan, J., Illeris, L., Soegaard, H., … Jonasson, S. (2000). Trace gas exchange in a high-Arctic valley: 1. Variationsin CO2 and CH4 Flux between tundra vegetation types. *Global Biogeochemical Cycles*, *14*(3), 701–713. https://doi.org/10.1029/1999GB001134

Christensen, Torben R, Ekberg, A., Ström, L., Mastepanov, M., Panikov, N., Öquist, M., … Oskarsson, H. (2003). Factors controlling large scale variations in methane emissions from wetlands. *Geophysical Research Letters*, *30*(7). https://doi.org/10.1029/2002GL016848

Deng, J., Li, C., Frolking, S., Zhang, Y., Bäckstrand, K., & Crill, P. (2014). Assessing effects of permafrost thaw on C fluxes based on multiyear modeling across a permafrost thaw gradient at Stordalen, Sweden. *Biogeosciences*, *11*(17), 4753–4770. https://doi.org/10.5194/bg-11-4753-2014

Dengel, S., Zona, D., Sachs, T., Aurela, M., Jammet, M., Parmentier, F. J. W., … Vesala, T. (2013). Testing the applicability of neural networks as a gap-filling method using CH4 flux data from high latitude wetlands. *Biogeosciences*, *10*(12), 8185–8200. https://doi.org/10.5194/bg-10-8185-2013

Dlugokencky, E. J., Nisbet, E. G., Fisher, R., & Lowry, D. (2011). Global atmospheric methane: budget, changes and dangers. *Philosophical Transactions of the Royal Society A: Mathematical, Physical and Engineering Sciences*, *369*(1943), 2058–2072. https://doi.org/10.1098/rsta.2010.0341

Dobson 1945-, A. J. (2002). *An introduction to generalized linear models / Annette J. Dobson*. Boca Raton: Chapman & Hall/CRC.

Falge, E., Baldocchi, D., Olson, R., Anthoni, P., Aubinet, M., Bernhofer, C., … Wofsy, S. (2001). Gap filling strategies for defensible annual sums of net ecosystem exchange. *Agricultural and Forest Meteorology*, *107*(1), 43–69. https://doi.org/10.1016/S0168-1923(00)00225-2

Godin, A., McLaughlin, J. W., Webster, K. L., Packalen, M., & Basiliko, N. (2012). Methane and methanogen community dynamics across a boreal peatland nutrient gradient. *Soil Biology and Biochemistry*, *48*, 96–105. https://doi.org/https://doi.org/10.1016/j.soilbio.2012.01.018

Intergovernmental Panel on Climate Change (Ed.). (2014). Anthropogenic and Natural Radiative Forcing. In *Climate Change 2013 – The Physical Science Basis: Working Group I Contribution to the Fifth Assessment Report of the Intergovernmental Panel on Climate Change* (pp. 659–740). https://doi.org/DOI: 10.1017/CBO9781107415324.018

Jackowicz-Korczyński, M., Christensen, T. R., Bäckstrand, K., Crill, P., Friborg, T., Mastepanov, M., & Ström, L. (2010). Annual cycle of methane emission from a subarctic peatland. *Journal of Geophysical Research: Biogeosciences*, *115*(G2). https://doi.org/10.1029/2008JG000913

Jammet, M, Dengel, S., Kettner, E., Parmentier, F.-J. W., Wik, M., Crill, P., & Friborg, T. (2017). Year-round CH4 and CO2 flux dynamics in two contrasting freshwater ecosystems of the subarctic. *Biogeosciences*, *14*(22), 5189–5216. https://doi.org/10.5194/bg-14-5189-2017

Jammet, M., Crill, P., Dengel, S., & Friborg, T. (2015). Large methane emissions from a subarctic lake during spring thaw: Mechanisms and landscape significance. *Journal of Geophysical Research: Biogeosciences*, *120*(11), 2289–2305. https://doi.org/10.1002/2015JG003137

Johansson, T., Malmer, N., Crill, P. M., Friborg, T., Åkerman, J. H., Mastepanov, M., & Christensen, T. R. (2006). Decadal vegetation changes in a northern peatland, greenhouse gas fluxes and net radiative forcing. *Global Change Biology*, *12*(12), 2352–2369. https://doi.org/10.1111/j.1365-2486.2006.01267.x

Kirschke, S., Bousquet, P., Ciais, P., Saunois, M., Canadell, J. G., Dlugokencky, E. J., … Zeng, G. (2013). Three decades of global methane sources and sinks. *Nature Geoscience*, *6*(10), 813–823. https://doi.org/10.1038/ngeo1955

Kljun, N., Calanca, P., Rotach, M. W., & Schmid, H. P. (2015). A simple two-dimensional parameterisation for Flux Footprint Prediction (FFP). *Geosci. Model Dev.*, *8*(11), 3695–3713. https://doi.org/10.5194/gmd-8-3695-2015

Knox, S. H., Matthes, J. H., Sturtevant, C., Oikawa, P. Y., Verfaillie, J., & Baldocchi, D. (2016). Biophysical controls on interannual variability in ecosystem-scale CO2 and CH4 exchange in a California rice paddy. *Journal of Geophysical Research: Biogeosciences*, *121*(3), 978–1001. https://doi.org/10.1002/2015JG003247

Kowalska, N., Chojnicki, B., Rinne, J., Haapanala, S., Siedlecki, P., Urbaniak, M., … Olejnik, J. (2013). Measurements of methane emission from a temperate wetland by eddy covariance method. *International Agrophysics*, *27*, 283–290. https://doi.org/10.2478/v10247-012-0096-5

Levenberg, K. (1944). A method for the solution of certain non-linear problems in least squares. *Quarterly of Applied Mathematics*, *2*(2), 164–168. Retrieved from http://www.jstor.org/stable/43633451

Li, T., Raivonen, M., Alekseychik, P., Aurela, M., Lohila, A., Zheng, X., … Zhang, W. (2016). Importance of vegetation classes in modeling CH4 emissions from boreal and subarctic wetlands in Finland. *Science of The Total Environment*, *572*, 1111–1122. https://doi.org/https://doi.org/10.1016/j.scitotenv.2016.08.020

Malmer, N., Johansson, T., Olsrud, M., & Christensen, T. R. (2005). Vegetation, climatic changes and net carbon sequestration in a North-Scandinavian subarctic mire over 30 years. *Global Change Biology*, *11*(11), 1895–1909. https://doi.org/10.1111/j.1365-2486.2005.01042.x

Marquardt, D. W. (1963). An Algorithm for Least-Squares Estimation of Nonlinear Parameters. *Journal of the Society for Industrial and Applied Mathematics*, *11*(2), 431–441. Retrieved from http://www.jstor.org/stable/2098941

Mastepanov, M, Sigsgaard, C., Tagesson, T., Ström, L., Tamstorf, M. P., Lund, M., & Christensen, T. R. (2013). Revisiting factors controlling methane emissions from high-Arctic tundra. *Biogeosciences*, *10*(7), 5139–5158. https://doi.org/10.5194/bg-10-5139-2013

Mastepanov, Mikhail, Sigsgaard, C., Dlugokencky, E. J., Houweling, S., Ström, L., Tamstorf, M. P., & Christensen, T. R. (2008). Large tundra methane burst during onset of freezing. *Nature*, *456*(7222), 628–630. https://doi.org/10.1038/nature07464

Mauder, M., & Foken, T. (2011). Documentation and Instruction Manual of the Eddy Covariance Software Package TK2. *Arbeitsergebnisse, Universität Bayreuth, Abteilung Mikrometeorologie, ISSN 1614-8916*, *46*. https://doi.org/10.5194/bg-5-451-2008

McCalley, C. K., Woodcroft, B. J., Hodgkins, S. B., Wehr, R. A., Kim, E.-H., Mondav, R., … Saleska, S. R. (2014). Methane dynamics regulated by microbial community response to permafrost thaw. *Nature*, *514*(7523), 478–481. https://doi.org/10.1038/nature13798

Mikhaylov, O. A., Miglovets, M. N., & Zagirova, S. V. (2015). Vertical methane fluxes in mesooligotrophic boreal peatland in European Northeast Russia. *Contemporary Problems of Ecology*, *8*(3), 368–375. https://doi.org/10.1134/S1995425515030099

NILSSON, M., SAGERFORS, J., BUFFAM, I., LAUDON, H., ERIKSSON, T., GRELLE, A., … LINDROTH, A. (2008). Contemporary carbon accumulation in a boreal oligotrophic minerogenic mire – a significant sink after accounting for all C-fluxes. *Global Change Biology*, *14*(10), 2317–2332. https://doi.org/10.1111/j.1365-2486.2008.01654.x

Nisbet, E G, Dlugokencky, E. J., Manning, M. R., Lowry, D., Fisher, R. E., France, J. L., … Ganesan, A. L. (2016). Rising atmospheric methane: 2007–2014 growth and isotopic shift. *Global Biogeochemical Cycles*, *30*(9), 1356–1370. https://doi.org/10.1002/2016GB005406

Nisbet, Euan G, Dlugokencky, E. J., & Bousquet, P. (2014). Methane on the Rise—Again. *Science*, *343*(6170), 493 LP – 495. https://doi.org/10.1126/science.1247828

Post, E., Alley, R. B., Christensen, T. R., Macias-Fauria, M., Forbes, B. C., Gooseff, M. N., … Wang, M. (2019). The polar regions in a 2{\textdegree}C warmer world. *Science Advances*, *5*(12).

https://doi.org/10.1126/sciadv.aaw9883

Pugh, C. A., Reed, D. E., Desai, A. R., & Sulman, B. N. (2018). Wetland flux controls: how does interacting water table levels and temperature influence carbon dioxide and methane fluxes in northern Wisconsin? *Biogeochemistry*, *137*(1), 15–25. https://doi.org/10.1007/s10533-017-0414-x

Raz-Yaseef, N., Torn, M. S., Wu, Y., Billesbach, D. P., Liljedahl, A. K., Kneafsey, T. J., … Wullschleger, S. D. (2017). Large CO2 and CH4 emissions from polygonal tundra during spring thaw in northern Alaska. *Geophysical Research Letters*, *44*(1), 504–513. https://doi.org/10.1002/2016GL071220

Rebmann, C., Aubinet, M., Schmid, H., Arriga, N., Aurela, M., Burba, G., … Franz, D. (2018). ICOS eddy covariance flux-station site setup: A review. *International Agrophysics*, *32*, 471–494. https://doi.org/10.1515/intag-2017-0044

Rinne, J, Tuovinen, J.-P., Klemedtsson, L., Aurela, M., Holst, J., Lohila, A., … Nilsson, M. B. (2020). Effect of the 2018 European drought on methane and carbon dioxide exchange of northern mire ecosystems. *Philosophical Transactions of the Royal Society B: Biological Sciences*, *375*(1810), 20190517. https://doi.org/10.1098/rstb.2019.0517

Rinne, Janne, Riutta, T., Pihlatie, M., Aurela, M., Haapanala, S., Tuovinen, J.-P., … Vesala, T. (2007). Annual cycle of methane emission from a boreal fen measured by the eddy covariance technique. *Tellus B: Chemical and Physical Meteorology*, *59*(3), 449–457. https://doi.org/10.1111/j.1600-0889.2007.00261.x

Rinne, Janne, Tuittila, E.-S., Peltola, O., Li, X., Raivonen, M., Alekseychik, P., … Vesala, T. (2018). Temporal Variation of Ecosystem Scale Methane Emission From a Boreal Fen in Relation to Temperature, Water Table Position, and Carbon Dioxide Fluxes. *Global Biogeochemical Cycles*, *32*(7), 1087–1106. https://doi.org/10.1029/2017GB005747

Saunois, M., Stavert, A. R., Poulter, B., Bousquet, P., Canadell, J. G., Jackson, R. B., … Zhuang, Q. (2020). The Global Methane Budget 2000--2017. *Earth System Science Data*, *12*(3), 1561–1623. https://doi.org/10.5194/essd-12-1561-2020

Song, C., Xu, X., Sun, X., Tian, H., Sun, L., Miao, Y., … Guo, Y. (2012). Large methane emission upon spring thaw from natural wetlands in the northern permafrost region. *Environmental Research Letters*, *7*(3), 034009. https://doi.org/10.1088/1748-9326/7/3/034009

Sturtevant, C. S., Oechel, W. C., Zona, D., Kim, Y., & Emerson, C. E. (2012). Soil moisture control over autumn season methane flux, Arctic Coastal Plain of Alaska. *Biogeosciences*, *9*(4), 1423–1440. https://doi.org/10.5194/bg-9-1423-2012

Taylor, M. A., Celis, G., Ledman, J. D., Bracho, R., & Schuur, E. A. G. (2018). Methane Efflux Measured by Eddy Covariance in Alaskan Upland Tundra Undergoing Permafrost Degradation. *Journal of Geophysical Research: Biogeosciences*, *123*(9), 2695–2710. https://doi.org/10.1029/2018JG004444

Turetsky, M. R., Kotowska, A., Bubier, J., Dise, N. B., Crill, P., Hornibrook, E. R. C., … Wilmking,

M. (2014). A synthesis of methane emissions from 71 northern, temperate, and subtropical wetlands. *Global Change Biology*, *20*(7), 2183–2197. https://doi.org/10.1111/gcb.12580

Verma, S. B., Baldocchi, D. D., Anderson, D. E., Matt, D. R., & Clement, R. J. (1986). Eddy fluxes of CO2, water vapor, and sensible heat over a deciduous forest. *Boundary-Layer Meteorology*, *36*(1), 71–91. https://doi.org/10.1007/BF00117459

Wutzler, T., Lucas-Moffat, A., Migliavacca, M., Knauer, J., Sickel, K., Šigut, L., … Reichstein, M. (2018). Basic and extensible post-processing of eddy covariance flux data with REddyProc. *Biogeosciences*, *15*(16), 5015–5030. https://doi.org/10.5194/bg-15-5015-2018

Yamulki, S., Anderson, R., Peace, A., & Morison, J. I. L. (2013). Soil CO2 CH4 and N2O fluxes from an afforested lowland raised peatbog in Scotland: implications for drainage and restoration. *Biogeosciences*, *10*(2), 1051–1065. https://doi.org/10.5194/bg-10-1051-2013

Zhang, Z., Zimmermann, N. E., Stenke, A., Li, X., Hodson, E. L., Zhu, G., … Poulter, B. (2017). Emerging role of wetland methane emissions in driving 21st century climate change. *Proceedings of the National Academy of Sciences*, *114*(36), 9647–9652. https://doi.org/10.1073/pnas.1618765114